ACS OMEGA

http://pubs.acs.org/journal/acsodf

Article

Structure Modification of Ginsenoside Rh_2 and Cytostatic Activity on Cancer Cells

Junyu Liang,[†] Xiaodong Tang,[†] Shanhe Wan, Jiayin Guo, Peng Zhao,* and Ling Lu*

Cite This: *ACS Omega* 2023, 8, 17245−17253

Read Online

ACCESS | Metrics & More | Article Recommendations | Supporting Information

ABSTRACT: Ginsenoside Rh_2 (Rh_2) is one of the most effective anticancer components extracted from red ginseng, but the poor solubility limits its clinical application. In this paper, ginsenoside Rh_2 was modified with maleimidocaproic acid or maleimidoundecanoic acid with functional groups at both ends. The structures of derivatives were determined by analysis of 1D and 2D nuclear magnetic resonance, Fourier transform infrared, and high-resolution mass spectrometry. Antiproliferative cell experiments showed that Rh_2 modified with maleimidocaproic acid (C−Rh_2) displayed higher cytostatic activity against different tumor cells compared with Rh_2, while Rh_2 modified with maleimidoundecanoic acid (U−Rh_2) did not exhibit obvious cytotoxicity. The results suggest that the length of the spacer arm may play an important role in the cytostatic activity of the Rh_2 derivatives.

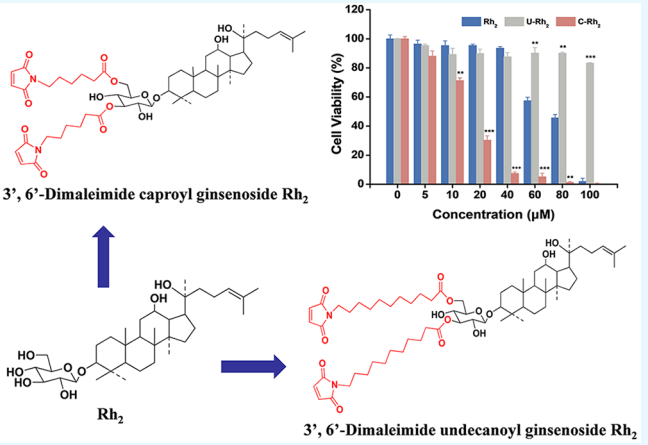

INTRODUCTION

Ginseng has been used as a multipotent herbal medicine in East Asian countries (such as Korea, Japan, and China).[1] Many studies show that ginsenosides, especially triterpene saponins, are the main active ingredients in ginseng, which are composed of ginsengenin and sugar through an ether bond.[2] Among them, ginsenoside Rh_2 (Rh_2) (Figure 1) has been adequately

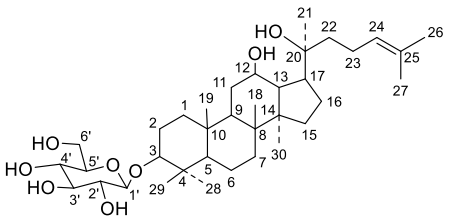

Figure 1. Structure of Rh_2.

investigated and exhibits remarkable functions including antitumor, anti-inflammatory, and antiallergic effects and enhancement of immune activity.[3−6] It is widely used to resist liver cancer, leukemia, cervical cancer, prostate cancer, colon cancer, breast cancer, etc.[7−12] Several recognized anticancer mechanisms of Rh_2 include (1) inducing apoptosis and autophagy of cancer cells;[13] (2) triggering cycle arrest of cancer cells;[14] (3) inhibiting invasion, migration, and metastasis of cancer cells;[15,16] and (4) suppressing angiogenesis and epithelial−mesenchymal transition (EMT).[17,18]

However, despite the advantages mentioned above, the clinical application of Rh_2 has been hampered due to its low solubility and difficulty in absorption.[19] Therefore, chemical structure modification (sulfation, esterification, acetylation, etc.) on ginsenosides has been carried out to improve the bioavailability and antitumor efficacy.[20−23] Maleimide aliphatic acids are a class of pharmaceutical intermediate with hydrophilic functional groups at both ends.[24,25] In our work, two maleimide fatty acids with different carbon chain lengths, namely, 6-maleimidocaproic acid and 11-maleimidoundecanoic acid, were attached to Rh_2, respectively, through the reaction between carboxyl groups in maleimide fatty acid and hydroxy groups in Rh_2 to improve the disadvantages of Rh_2. The junction sites and numbers were characterized using nuclear magnetic resonance (NMR), Fourier transform infrared (FTIR), and high-resolution mass spectrometry (HRMS). The effect of the length of the spacer arm on the antiproliferative activity of Rh_2 derivatives was preliminarily investigated.

Received: March 16, 2023
Accepted: April 18, 2023
Published: May 1, 2023

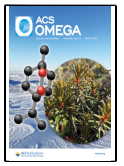

Scheme 1. Synthesis of Rh_2 Derivatives (C−Rh_2 and U−Rh_2)

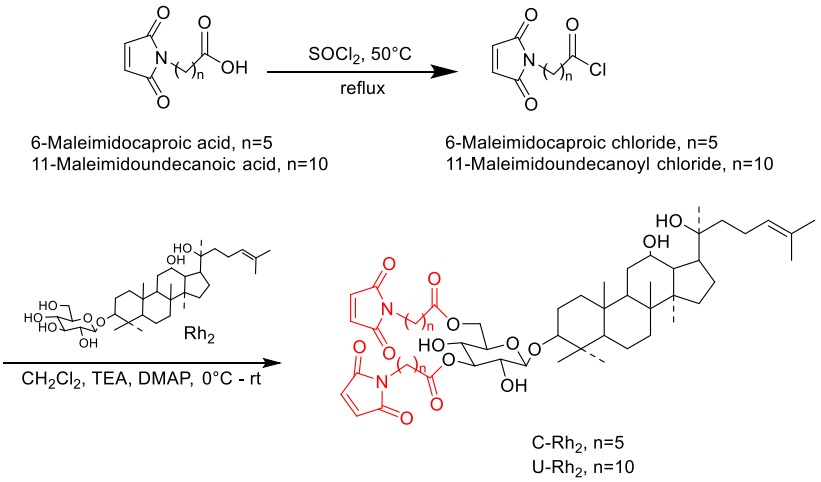

RESULTS AND DISCUSSION

Synthesis and Characterization of Rh_2 Derivatives. 6-Maleimidocaproic acid-modified Rh_2 (C−Rh_2) and 11-maleimidoundecanoic acid-modified Rh_2 (U−Rh_2) were synthesized and purified as described in the Experimental Section (Scheme 1), and the structures were elucidated using a combination of FTIR, NMR, and HRMS.

C−Rh_2 was isolated as a white powder. The molecular formula of C−Rh_2 was deduced as $C_{56}H_{84}N_2O_{14}$ on the basis of a protonated molecular ion peak at m/z 1009.5989 $[M + H]^+$ in HRESIMS (calcd 1009.5995, Figure S12, Supporting Information), suggesting that there were 2 equiv of 6-maleimidocaproic acid molecules connected to Rh_2. The FTIR spectrum (Figure S13, Supporting Information) displayed absorption bands characterized as the hydroxyl group (3100−3500 cm^{-1}), carbonyl group (1706 cm^{-1}), and carbon−carbon double bond (1628 cm^{-1}), whereas out-of-plane bending vibration (γ_{O-H}, 948 cm^{-1}) of the hydroxyl group in the carboxyl group of 6-maleimidocaproic acid disappeared in C−Rh_2, indicating that the carboxyl group was converted to the ester group after 6-maleimidocaproic acid was linked onto Rh_2.

The ^1H NMR and ^{13}C NMR data of C−Rh_2 were similar to those of Rh_2 (Table 1 and Figures S6 and S7, Supporting Information), except that the signals corresponding to maleimide fatty acyl appeared (Table 1). The ^1H NMR spectrum of Rh_2 displayed signals ranging from δ_H 5.00 to 4.00 for protons in the glycogen moiety, δ_H 5.30 typical for the double bond, and δ_H less than 4.00 for protons in the ginsengenin portion. In the ^{13}C NMR data, the carbon signals of δ_C ranging from 107.46 to 63.55 were mainly corresponding to glycogen (except δ_C 89.26, 73.45, and 71.48 for C-3, C-20, and C-12 in ginsengenin, respectively), while the signals at δ_C 131.25 (C-25), 126.81 (C-24), and δ_C less than 60 were diagnostic for ginsengenin.

Besides the signals mentioned above, the ^1H NMR spectrum of C−Rh_2 (Table 1 and Figure S14, Supporting Information) exhibited signals at δ_H 6.82 (H-8″and H-9″), 3.50 (H-6″), 2.33 (H-2″), 1.59 (H-3″), 1.51 (H-5″), and 1.29 (H-4″) diagnostic for maleimide caproyl groups. In the ^{13}C NMR spectrum of C−Rh_2 (Table 1 and Figure S15, Supporting Information), signals associated with maleimide caproyl groups were split into two adjacent groups, namely, δ_C 173.85, 35.00, 25.26, 26.92, 28.96, 38.06, 171.75, and 134.87 (C-1″−8″) and δ_C 173.78, 34.66, 25.18, 26.78, 28.90, 38.02, 171.72, and 134.83 (another group of C-1″∼8″). This just indicated that two 6-maleimidocaproic acid molecules had connected onto Rh_2, which was consistent with the formula obtained by HRMS.

To figure out which two sites of Rh_2 the 6-maleimidocaproic acid molecules were connected to, the structure of C−Rh_2 was characterized by HSQC, $^1H-^1H$ COSY, and HMBC two-dimensional NMR. There were no significant changes in the δ_H and δ_C of C-12, C-20, and neighboring atoms, while the main changes of chemical shifts were observed at the glucose moiety, so we speculated that the esterification occurred on the glycogen ring. Since there was no hydroxyl group on C-1′ to participate in the reaction, so the chemical shifts of C-1′ (δ_C 107.46) and H-1′ (δ_H 4.97) were similar before and after esterification. The HSQC spectrum of C−Rh_2 (Figure S16, Supporting Information) showed that the δ_C value of C-6′ was 64.56, while the δ_H values of H-6′$_a$ and H-6′$_b$ downfield shifted to 4.99 and 4.79, respectively. Meanwhile, the cross-peak signals of H-6′$_a$ (δ_H 4.99) and H-6′$_b$ (δ_H 4.79) to C-1″ (δ_C 173.85 and 173.78) of ester carbonyl in maleimide caproyl groups were observed in the HMBC spectrum (Figure S17, Supporting Information), indicating that one of the 6-maleimidocaproic acid molecules was attached to C-6′ (Figure 2).

The coupling correlation between δ_H 4.07 and H-1′ (δ_H 4.89) in the $^1H-^1H$ COSY spectrum of C−Rh_2 (Figure S18, Supporting Information) suggested that δ_H 4.07 belonged to H-2′, and the cross-peak of H-2′ (δ_H 4.07) to carbon δ_C 73.81 in the HSQC spectrum implied that δ_C 73.81 could be assigned to C-2′. The presence of a signal at H-6′$_b$ (δ_H 4.79) and δ_H 4.10 in the $^1H-^1H$ COSY spectrum allowed the assignment of δ_H 4.10 to H-5′, and the correlation from H-5′ (δ_H 4.10) to δ_C 75.32 in HSQC further inferred that δ_C 75.32 was due to C-5′. In the HMBC spectrum, besides the correlationship between H-6′$_b$ and C-5′, the cross-peak of H-6′$_a$ (δ_H 4.99) to carbon δ_C 70.21 supported the assignment of δ_C 70.21 to C-4′, and then the signal from δ_H 4.12 to C-4′ (δ_C 70.21) in the HSQC spectrum provided evidence that δ_H 4.12 was due to H-4′. Finally, the HSQC cross-peak of the proton at δ_H 5.80 and carbon δ_C 79.43 should be assigned to H-3′ and C-3′, which was consistent with the H-3′ (δ_H 5.80) and H-4′ (δ_H 4.12) coupling observed in the $^1H-^1H$ COSY spectrum and the correlation signal from H-3′ (δ_H 5.80) to C-4′ (δ_C 70.21) and C-2′ (δ_C 73.81) in the HMBC spectrum.

https://doi.org/10.1021/acsomega.3c01665
ACS Omega 2023, 8, 17245−17253

Table 1. ^{13}C (100 MHz) and ^{1}H NMR (400 MHz) Data for Rh_2, C−Rh_2, and U−Rh_2 in Pyridine-d_5

	Rh_2		C−Rh_2		U−Rh_2	
position	δ_C, type	δ_H (J in Hz)	δ_C, type	δ_H (J in Hz)	δ_C, type	δ_H, type
C-1	40.17, CH_2	1.48, m	40.10, CH_2	1.43, m	40.12, CH_2	1.53, m
		0.78, s		0.84, s		0.82, s
C-2	27.34, CH_2	2.24, dd (13.6, 3.5)	27.32, CH_2	2.22, d (11.9)	27.34, CH_2	2.24, d (9.7)
		1.83, m		1.90, m		1.92, m
C-3	89.26, CH	3.38, dd (11.5, 4.5)	89.90, CH	3.34, dd (11.5, 4.1)	89.93, CH	3.36, dd (11.6, 4.1)
C-4	40.49, C		40.50, C		40.53, C	
C-5	56.85, CH	0.74, d (11.5)	56.85, CH	0.79, d (10.8)	56.93, CH	0.82, d (10.8)
C-6	18.94, CH_2	1.48, m	18.92, CH_2	1.47, m	18.95, CH_2	1.53, m
		1.36, m		1.33, m		1.41, m
C-7	35.64, CH_2	1.48, m	35.60, CH_2	1.51, m	35.64, CH_2	1.53, m
		1.21, m		1.22, m		1.28, m
C-8	37.44, C		37.49, C		37.52, C	
C-9	50.86, CH	1.40, m	50.91, CH	1.48, m	50.96, CH	1.44, m
C-10	39.61, C		39.71, C		39.78, C	
C-11	32.55, CH_2	2.05, m	32.52, CH_2	2.10, m	32.54, CH_2	2.10, m
		1.51, m		1.52, m		1.53, m
C-12	71.48, CH	3.91, m	71.46, CH	3.92, m	71.46, CH	3.92, m
C-13	49.04 CH	2.02, m	49.06, CH	2.04, m	49.08, CH	2.07, m
C-14	52.19, C		52.19, C		52.19, C	
C-15	31.83, CH_2	1.54, m	31.81, CH_2	1.51, m	31.83, CH_2	1.55, m
		1.05, m		1.06, m		1.08, m
C-16	27.21, CH_2	1.90, m	27.16, CH_2	1.90, m	27.19, CH_2	1.92, m
		1.42, m		1.43, m		1.38, m
C-17	55.29, CH	2.35, dd (10.5, 3.5)	55.30, CH	2.38, m	55.30, CH	2.37, m
C-18	16.32, CH_3	0.95, s	16.31, CH_3	0.96, s	16.34, CH_3	1.00, s
C-19	16.86, CH_3	0.78, s	16.84, CH_3	0.84, s	16.86, CH_3	0.82, s
C-20	73.45, C		73.44, C		73.45, C	
C-21	27.57, CH_3	1.42, s	27.54, CH_3	1.43, s	27.57, CH_3	1.44, s
C-22	36.37, CH_2	2.03, m	36.33, CH_2	2.04, m	36.35, CH_2	2.05, m
		1.68, m		1.69, m		1.69, m
C-23	23.48, CH_2	2.59, m	23.47, CH_2	2.60, m	23.48, CH_2	2.59, m
		2.27, m		2.28, m		2.27, m
C-24	126.81, CH	5.30, t (7.0)	126.79, CH	5.31, t (7.1)	126.80, CH	5.32, t (7.2)
C-25	131.25, C		131.25, C		131.24, C	
C-26	26.33, CH_3	1.63, s	26.33, CH_3	1.66, s	26.33, CH_3	1.57, s
C-27	18.19, CH_3	1.61, s	18.18, CH_3	1.60, s	18.20, CH_3	1.64, s
C-28	28.65, CH_3	1.34, s	28.52, CH_3	1.33, s	28.53, CH_3	1.27, s
C-29	17.51, CH_3	0.98, s	17.49, CH_3	0.94, s	17.51, CH_3	0.94, s
C-30	17.30, CH_3	0.95, s	17.16, CH_3	0.98, s	17.16, CH_3	0.98, s
1′	107.46, CH	4.97, d (7.5)	107.18, CH	4.89, d (7.5)	107.24, CH	4.90, d (7.7)
2′	76.28, CH	4.06, m	73.81 CH	4.07, m	73.87, CH	4.08, m
3′	79.25, CH	4.25, m	79.43, CH	5.80, m	79.41, CH	5.86, m
4′	72.34, CH	4.23, m	70.21, CH	4.12, m	70.33, CH	4.14, m
5′	78.88, CH	4.03, m	75.32, CH	4.10, m	75.37, CH	4.10, m
6′	63.55, CH_2	4.61, dd (7.5, 2.5)	64.56, CH_2	4.99, d (11.4)	64.59, CH_2	5.04, d (11.5)
		4.42, dd (11.5, 5.5)		4.79, d (6.4)		4.83, dd (11.6, 5.1)
1″			173.85, C		174.11, C	
			173.78, C		174.04, C	
2″			35.00, CH_2	2.33, t (7.7)	35.30 CH_2	2.40, t (7.4)
			34.66, CH_2		34.95 CH_2	
3″			25.26, CH_2	1.59, m	25.86 CH_2	1.67, m
			25.18, CH_2		25.80 CH_2	
4″			26.92, CH_2	1.29, m	30.19, CH_2	1.27, m
			26.78, CH_2		29.97, CH_2	
5″			28.96, CH_2	1.51, m	29.87, CH_2	1.18−1.25, m
			28.90, CH_2		29.84, CH_2	
6″			38.06, CH_2	3.50, s	30.14, CH_2	1.18−1.25, m
			38.02, CH_2		30.10, CH_2	
7″			171.75, C		30.02, CH_2	1.18−1.25, m

https://doi.org/10.1021/acsomega.3c01665
ACS Omega 2023, 8, 17245−17253

Table 1. continued

	Rh_2		C−Rh_2		U−Rh_2	
position	δ_C, type	δ_H (J in Hz)	δ_C, type	δ_H (J in Hz)	δ_C, type	δ_H, type
			171.72, C		30.00, CH_2	
8″			134.87, CH	6.82, s	29.76, CH_2	1.18−1.25, m
			134.83, CH			
9″			134.87, CH	6.82, s	27.49, CH_2	1.18, m
			134.83, CH		27.43, CH_2	
10″			171.75, C		29.34, CH_2	1.57, m
			171.72, C		29.30, CH_2	
11″					38.35, CH_2	3.54, t (6.8)
					38.33, CH_2	
12″					171.83, C	
13″					134.90, CH	6.87, s
14″					134.90, CH	6.87, s
15″					171.83, C	

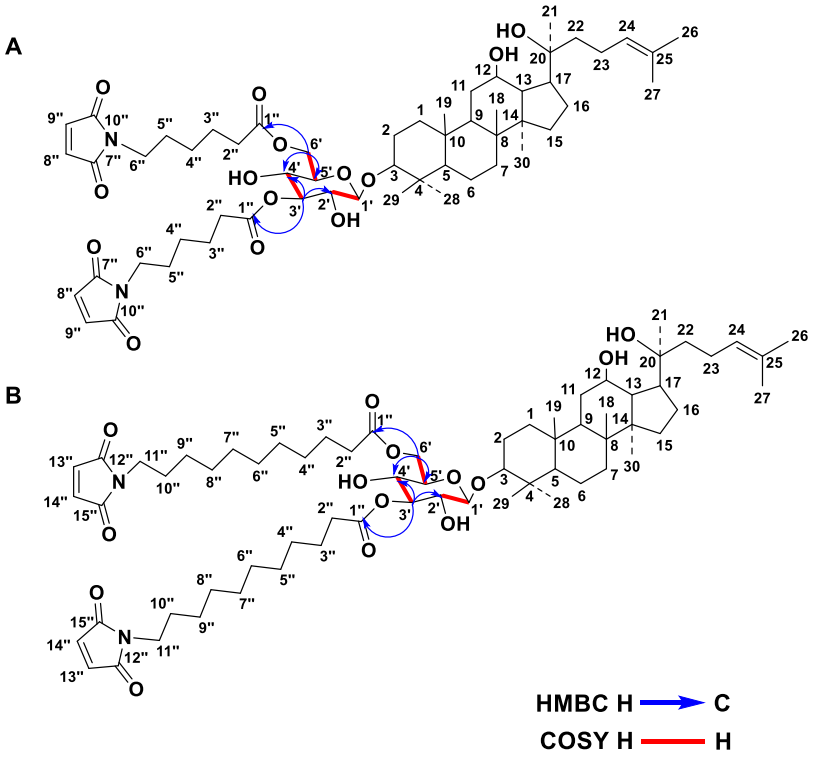

Figure 2. Selected HMBC and COSY correlations of C−Rh_2 (A) and U−Rh_2 (B).

Furthermore, the cross-peak signal of H-3′ (δ_H 5.80) and C-1″ (δ_C 173.78) of the ester carbonyl in the maleimide caproyl group in the HMBC spectrum indicated that the second 6-maleimidocaproic acid molecule was attached to C-3′ in the glucose ring (Figure 2).

According to the attribution of carbon and proton signals in 2D NMR discussed above, 6-maleimidocaproic acid was connected to C-3′ and C-6′ of the glucose moiety of Rh_2; thus, C−Rh_2 finally elucidated as 3′,6′-dimaleimide caproyl ginsenoside Rh_2. The introduction of acyl groups onto the glucose moiety caused a significant downfield shift of the proton attached to acyl-linked carbon; therefore, the proton signals of H-3′ and H-6′ shifted about 1.55 and 0.38 ppm, respectively. Meanwhile, the carbon signals for C-2′, C-4′, and C-5′ adjacent to the reaction site upfield shifted to δ_C 73.81, 70.21, and 75.32, respectively.

U−Rh_2 was obtained as an amorphous solid and assigned the molecular formula $C_{66}H_{104}N_2O_{14}$ based on HREISMS ([M + H]$^+$ at m/z 1149.7555, calcd 1149.7560, Figure S19, Supporting Information). This molecular formula inferred two equivalent maleimide undecanoyl groups in U−Rh_2. The FTIR absorption bands at 3100−3500, 1707, and 1629 cm^{-1} indicated the presence of the hydroxyl group, carbonyl group, and carbon−carbon double bond. The disappearance of γ_{O-H} in carboxy (950 cm^{-1}) confirmed the conversion of carboxyl to ester group after 11-maleimidoundecanoic acid was linked to Rh_2.

The NMR spectroscopic data of U−Rh_2 resembled those of Rh_2 and C−Rh_2, except for new signals associated with 11-maleimidoundecanoic acid. The ^{1}H NMR spectrum (Figure S20, Supporting Information) exhibited signals at δ_H 6.87 (H-13″ and H-14″), 3.54 (H-11″), 2.40 (H-2″), 1.67 (H-3″), 1.57 (H-10″), 1.27 (H-4″), and 1.18 (H-9″) due to maleimide

https://doi.org/10.1021/acsomega.3c01665
ACS Omega 2023, 8, 17245−17253

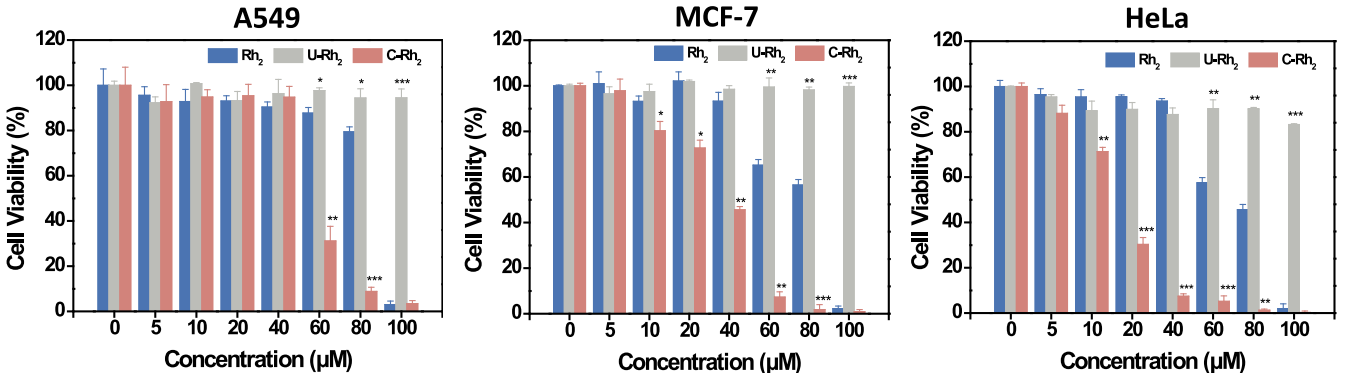

Figure 3. Inhibition of the proliferation of A549, MCF-7, and HeLa cells by Rh_2, C−Rh_2, and U−Rh_2 with different concentrations (5, 10, 20, 40, 60, 80, and 100 μM) assessed using the MTT assay. All data are presented as means ± SD of three independent experiments. *$p < 0.05$, **$p < 0.01$, and ***$p < 0.001$ vs Rh_2 group.

undecanoyl groups. In the ^{13}C NMR spectrum (Figure S21, Supporting Information), two sets of very close signals of δ_C 174.11, 35.30, 25.86, 30.19, 29.87, 30.14, 30.02, 29.76, 27.49, 29.34, 38.35, 171.83, and 134.90 (C-1″−13″) and δ_C 174.04, 34.95, 25.80, 29.97, 29.84, 30.10, 30.00, 29.76, 27.43, 29.30, 38.33, 171.83, and 134.90 (another group of C-1″−13″) were observed, suggesting that two 11-maleimidoundecanoic acid molecules were grafted onto Rh_2.

Similarly, in the ^1H NMR spectrum of U−Rh_2, the proton signals downfield shifts of δ_H 5.86 (H-3′) and 5.04/4.83 (H-6′$_a$/6′$_b$) were observed. While in the ^{13}C NMR spectrum, the carbon signals at δ_C 73.87 (C-2′), 70.33 (C-4′), and 75.37 (C-5′) were shifted upfield compared with δ_C 76.28, 72.34 and 78.88 in Rh_2. These indicated that 11-maleimidoundecanoic acid molecules were also connected to C-3′ and C-6′ of Rh_2. Further, this conclusion could be confirmed by the analysis of HSQC, $^1H-^1H$ COSY, and HMBC spectra (Figures S22−24, Supporting Information). In brief, the correlation signals between H-6′$_a$/6′$_b$ (δ_H 5.04/4.83) on the glucose moiety and C-1″ (δ_C 174.04) in the maleimide undecanoyl group, as well as the signal between H-3′ (δ_H 5.86) and C-1″ (δ_C 174.11) in the HMBC spectrum, also provided evidence that U−Rh_2 could be elucidated as 3′,6′-dimaleimide undecanoyl ginsenoside Rh_2.

To evaluate the solubility property of Rh_2 modified with maleimide fatty acids, the oil−water partition coefficient and solubility were measured. The results showed that the values of oil−water partition coefficient log P were 3.48 for Rh_2, 2.27 for C−Rh_2, and 2.84 for U−Rh_2. The solubility of Rh_2, C−Rh_2, and U−Rh_2 in water was 74.04, 292.06, and 162.69 $\mu g \cdot mL^{-1}$, respectively. That is, the solubility of C−Rh_2 and U−Rh_2 increased to approximately 4 and 2 times, respectively, compared with Rh_2. These indicate that the derivatives modified with maleimide fatty acids exhibit better solubility property compared with Rh_2 and are expected to show better bio-absorption performance. The stability test showed that there was no peak shift or other changes in the ^1H NMR spectra within 144 h in an alkaline medium, indicating that C−Rh_2 and U−Rh_2 were relatively stable (Figure S25, Supporting Information).

In Vitro Antiproliferative Activity of the Rh_2 Derivatives. To investigate the in vitro cytostatic activity of Rh_2 derivatives, A549, HeLa, and MCF-7 cells were treated with Rh_2, C−Rh_2, and U−Rh_2 at different concentrations (Figure 3). The MTT assay showed that the IC_{50} values for Rh_2 on A549, MCF-7, and HeLa cells were 85.26, 73.58, and 67.95 μM, respectively, while for C−Rh_2, the IC_{50} values were 54.82, 29.80, and 14.17 μM. In other words, the cytotoxicity of C−Rh_2 against A549, MCF-7, and HeLa cell lines was approximately 1.6, 2.5, and 4.8 times that of Rh_2, respectively. It can also be seen from Figure 3 that C−Rh_2 had the highest cytostatic activity against the HeLa cell line, which was also proved by the live/dead cell staining assay (Figure S26, Supporting Information). However, U−Rh_2 exhibited only slight cytotoxicity to the HeLa cell line and no cytotoxicity to the other two cells. The structural difference between C−Rh_2 and U−Rh_2 is the number of carbon atoms on the acyl side chain, so it could be inferred that the length of the spacer arm might have a significant effect on the antiproliferative activity of Rh_2 derivatives. Further research would be carried out to illustrate this issue. Since C−Rh_2 showed better cytotoxicity to tumor cells, it would be discussed in more detail hereinafter.

The Annexin V/PI apoptosis assay by flow cytometry showed that the percentage of early and late apoptosis in the control group and Rh_2-treated group was 6.2 and 5.3%, respectively, while it increased to 36.4% for the C−Rh_2 treated group (Figure 4A). These results suggested that C−Rh_2 demonstrated greater effectiveness in inducing apoptosis than Rh_2 in HeLa cells.

The JC-1 dye was used to examine the change of mitochondrial membrane potential. The JC-1 dye enters and accumulates in the energized and negatively charged mitochondria and spontaneously forms red fluorescent J-aggregates in healthy cells but retains its original green fluorescence in unhealthy or apoptotic cells.[26] Compared with the control group, the reduction of red fluorescence and the increase of green fluorescence in the C−Rh_2-treated group were more remarkable than those in the Rh_2-treated group (Figure 4B). This indicated that C−Rh_2 treatment induced severer damage to mitochondria than Rh_2 in HeLa cells.

The increase of intracellular ROS can result in mitochondrial damage and play a significant role in pro-apoptotic activities.[27] To evaluate whether C−Rh_2 induced ROS accumulation in HeLa cells, DCFH-DA staining was conducted after treatment with Rh_2 and C−Rh_2. It was found that the C−Rh_2 treated group generated stronger DCF fluorescence intensity than the Rh_2-treated group at the same concentration (Figure 4C). Therefore, C−Rh_2 administration could produce more ROS than Rh_2 administration, suggesting that the increased ROS might be a critical reason for C−Rh_2 to inhibit HeLa cell growth.

https://doi.org/10.1021/acsomega.3c01665
ACS Omega 2023, 8, 17245−17253

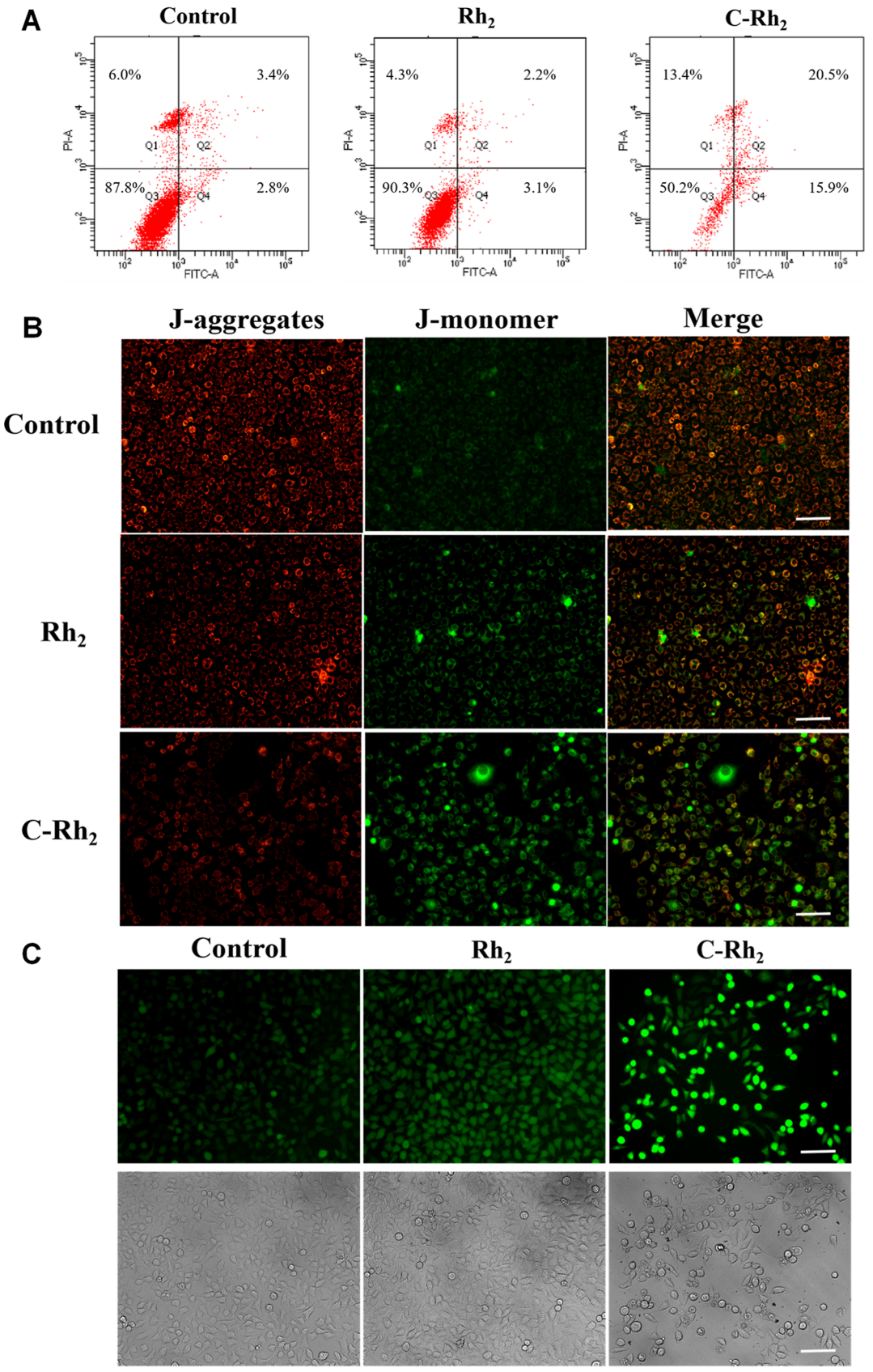

Figure 4. Analysis of the effects of C−Rh_2-induced HeLa cell apoptosis. (A) HeLa cells were treated with Rh_2 (20 μM) and C−Rh_2 (20 μM) for 24 h. Then, the cells were stained with annexin V-FITC and propidium iodide (PI) and finally analyzed by flow cytometry. (B) Cultures were treated with compounds aforementioned for 24 h and stained subsequently with the JC-1 dye. (C) The cells were treated with compounds for 24 h and then stained with a fluorescent probe DCFH-DA. Images were observed under an inverted fluorescent microscope (scale bar = 50 μm).

https://doi.org/10.1021/acsomega.3c01665
ACS Omega 2023, 8, 17245−17253

In conclusion, two derivatives of Rh_2 with better solubility were prepared by esterification of maleimide fatty acid with different lengths of spacer arms. The results of in vitro antiproliferative activity test showed that C−Rh_2 exhibited higher cytotoxicity against cancer cell lines compared with Rh_2, especially for HeLa cells, whereas U−Rh_2 with longer carbon chains showed little cytotoxicity. These results suggested that the spacer arm length may have an important effect on the antiproliferative activity of Rh_2 derivatives.

EXPERIMENTAL SECTION

Materials. Ginsenoside Rh_2 (Rh_2) was supplied by Nanjing Dilger Medical Technology Co., Ltd (Nanjing, China). 6-Maleimidocaproic acid and 11-maleimidoundecanoic acid were obtained from Macklin (Shanghai, China). 4-Dimethylaminopyridine (DMAP) was purchased from Aladdin (Shanghai, China).

General Experimental Procedures. FTIR spectra were recorded with a Nicolet 6700 FTIR spectrometer (Thermo, America). The ^1H and ^{13}C NMR spectra were recorded on a Bruker Avance III 400 NMR spectrometer in pyridine-d_5 with tetramethylsilane (TMS) as a reference. Chemical shifts (δ) are expressed in parts per million (ppm), with the coupling constants (J) reported in hertz (Hz). Ultraviolet−visible (UV−vis) absorption spectra were recorded using a UV-5500PC spectrophotometer (Metash, China). High-performance liquid chromatography (HPLC) measurements were carried out on a Shimadzu LC-20AT pump with a SIL-20A autosampler using a Kromasil 100-5-C18 column (250 mm × 4.6 mm i.d.). Detection was executed by a SPD-M20A photodiode array detector. HRMS data were obtained on an Orbitrap Fusion instrument in the ESI mode. Silica gel GF254 plates for thin-layer chromatography and silica gel (200−300 mesh) for column chromatography were produced by Qingdao Marine Chemical Factory.

Chemical Procedures for the Preparation of C−Rh_2 and U−Rh_2. In order to prepare the derivatives of Rh_2, 6-maleimidocaproic chloride and 11-maleimidoundecanoyl chloride were first synthesized by the reaction of 6-maleimidocaproic acid and 11-maleimidoundecanoic acid with $SOCl_2$ at 50 °C and refluxed for 3 h, respectively. Then, the obtained 6-maleimidocaproic chloride or 11-maleimidoundecanoyl chloride was reacted with Rh_2 in the presence of triethylamine (TEA) as an acid binding agent and 4-dimethyl aminopyridine (DMAP) as the catalyst, as illustrated in Scheme 1.

3′,6′-Dimaleimide Caproyl Ginsenoside Rh_2 (C−Rh_2). Rh_2 (168.1 mg, 0.27 mmol) and TEA (185 μL, 1.2 mmol) were dispersed in dry CH_2Cl_2 (4 mL); then, 6-maleimidocaproic chloride (229.1 mg, 1.00 mmol, 3.70 equiv) was added dropwise. The reaction mixture was stirred at 0 °C for 30 min; subsequently, DMAP (1.8 mg, 0.015 mmol, 0.05 equiv) was added. After 6 h, the mixture was diluted by adding CH_2Cl_2 (15 mL), and then a dilute hydrochloric acid solution (pH = 2, 2 × 20 mL) was added. After that, the mixture was layered with a separating funnel, and the water layer was discarded. The organic layer was washed successively with saturated aqueous $NaHCO_3$ (2 × 20 mL) and saturated aqueous NaCl (2 × 20 mL) and then dried by anhydrous Na_2SO_4 and filtered through a funnel. Finally, the filtered solution was concentrated under vacuum and then purified by column chromatography (30 to 60% EtOAc in petroleum ether) to yield C−Rh_2 as a white solid powder (107.9 mg, 0.11 mmol, 39.6%): R_f = 0.52 ($MeOH/CH_2Cl_2$ 1:17 v/v); IR (KBr) ν_{max} 3100−3500, 2934, 1706, 1628, 1402, 696 cm^{-1}; ^1H NMR and ^{13}C NMR data, see Table 1; HRESIMS m/z: 1009.5989 $[M + H]^+$ (calcd for $C_{56}H_{84}N_2O_{14}$, 1009.5995).

3′,6′-Dimaleimide Undecanoyl Ginsenoside Rh_2 (U−Rh_2). 11-Maleimidoundecanoyl chloride (299.2 mg, 1 mmol, 3.70 equiv) was added dropwise to an anhydrous CH_2Cl_2 (4 mL) solution of Rh_2 (168.1 mg, 0.27 mmol) and TEA (231 μL, 1.5 mmol) with magnetic stirring, and then DMAP (1.8 mg, 0.015 mmol, 0.05 equiv) was added after 30 min. The reaction mixture was stirred at 0 °C to room temperature for 6 h before being diluted with CH_2Cl_2 (15 mL). Next, dilute hydrochloric acid solution (20 mL) was added, resulting in phase separation. The collected organic phase was washed with saturated aqueous $NaHCO_3$ (20 mL) and saturated aqueous NaCl (20 mL) in turn. Following this, the organic phase was dried with anhydrous Na_2SO_4 and then evaporated under reduced pressure after filtering. Purification of the residue by column chromatography (20 to 50% EtOAc in petroleum ether) afforded U−Rh_2 as a pale yellow amorphous solid: R_f = 0.55 ($MeOH/CH_2Cl_2$ 1:17 v/v); IR (KRr) ν_{max} 3100−3500, 2929, 2856, 1707, 1629, 1402, 696 cm^{-1}; ^1H NMR and ^{13}C NMR data, see Table 1; HRESIMS m/z: 1149.7555 $[M + H]^+$ (calcd for $C_{66}H_{104}N_2O_{14}$, 1149.7560).

Determination of the Oil−Water Partition Coefficient. The oil−water partition coefficient was determined by the shake flask method. Rh_2, C−Rh_2, and U−Rh_2 were added into the pre-prepared water-saturated n-octanol solution, respectively, and dissolved ultrasonically. 1 mL of the solution was taken out and centrifuged at 10,000 rpm for 10 min. Then, the supernatant was diluted to measure its absorbance at 217 nm, and the concentration in the oil phase (C_0) was calculated using the standard curve method. Another 1 mL of the solution was added into 1 mL of water solution saturated with n-octanol. The mixture was oscillated at 37 °C for 24 h (100 rpm) to achieve dissolution equilibrium in the two phases. Subsequently, the mixture was centrifuged at 10,000 rpm for 10 min, and then the absorbance of the water phase (the lower layer) was measured, and the concentration in the water phase (C_w) was calculated. The oil−water partition coefficient was calculated according to the formula

$$P = (C_o - C_w)/C_w$$

Solubility Measurement. Excess Rh_2, C−Rh_2, and U−Rh_2 were added to 2 mL of distilled water, respectively, and oscillated for 24 h at 37 °C (100 rpm). The mixture was centrifuged at 10,000 rpm for 10 min, then the supernatant was taken, and the absorbance was measured at 217 nm. The solubility was calculated using the standard curve method.

Stability Test. C−Rh_2 and U−Rh_2 were dissolved, respectively, in pyridine-d_5 (0.5 mL). ^1H NMR scans were conducted at 0, 12, 24, 48, 72, and 144 h.

Cell Culture. All cells were cultured in DMEM (Gibco Life Technology Co., Ltd., USA) containing 10% (v/v) fetal bovine serum (Procell Life Science & Technology Co., Ltd.) and 1% (w/v) penicillin−streptomycin (Gibco Life Technology Co., Ltd.) at 37 °C in a humidified chamber supplemented with 5% CO_2. The culture media were replaced every 48 h, and the cultured cells were digested with 0.25% trypsin-EDTA solution when reached 80−90% confluency.

Cell Proliferation Activity Assay. For the evaluation of the cytostatic activities of Rh_2, C−Rh_2, and U−Rh_2, the cells were seeded at a density of 5 × 10^3 cells/well in 96-well flat-

https://doi.org/10.1021/acsomega.3c01665
ACS Omega 2023, 8, 17245−17253

bottomed plates. After incubation for 24 h, the cells were treated with the test compounds mentioned above (final concentration 5−100 μM) and simultaneously treated with 1‰ DMSO as a control group. Thereafter, the effect of the test compounds on the proliferation of tumor cells was assessed according to the 3-(4,5-dimethylthiazol-2-yl)-2, 5-diphenyltetrazolium bromide (MTT) method. The results were obtained on a multi-detection microplate reader (Tecan, Infinite M1000 PRO) using a wavelength of 490 nm. Data were presented as cell viability, and IC_{50} values were calculated using GraphPad Prism software (GraphPad Software, CA). In each MTT assay, every sample was tested in three to five replicates, and percent cell survival was calculated using the following equation

$$\text{Cell viability (\%)} = \text{absorbance of the experimental group/absorbance of the control group} \times 100\%$$

Flow Cytometry Analysis of Apoptosis. To evaluate the effect of C−Rh_2 on cell apoptosis, we performed a flow cytometry analysis. Briefly, HeLa cells were placed at a density of 5×10^5 cells/well in six-well plates with 3 mL of DMEM containing 10% (v/v) fetal bovine serum and 1% (w/v) penicillin−streptomycin and then incubated for 24 h. Next, the supernatants were replaced by fresh culture medium with Rh_2 (20 μM) and C−Rh_2 (20 μM) and incubated for 24 h. The cells were harvested and resuspended in a binding buffer after treatment. Annexin V-FITC and PI (Solarbio Science Co., Ltd.) were then added according to the manufacturer's instructions. Finally, the cell apoptosis rate was analyzed by a flow cytometer (FACSAria, Becton Dickinson, USA).

Mitochondrial Membrane Potential Assessment by JC-1 Staining. HeLa cells were seeded in six-well plates and treated with compounds described previously for 24 h. Then, the cells were stained with JC-1 according to the manufacturer's protocol. Last, the stained cells were captured using an inverted fluorescence microscope (Axio Observer A1, Germany).

Reactive Oxygen Species Measurement by DCFH-DA Staining. The cell culture and treatment processes were the same as described above. After that, the cells were stained with a ROS assay kit (containing DCFH-DA as the indicator) following the manufacturer's instructions. The green fluorescence was observed under a blue light with a fluorescence microscope.

Statistical Analysis. The results were shown as the mean ± standard deviation (SD) of at least three independently performed experimental measurements to avoid possible variation in cell cultures. Student's *t*-test was used, and $p < 0.05$ was considered to be statistically significant. Statistical significances were indicated with asterisks ($^*p < 0.05$, $^{**}p < 0.01$, and $^{***}p < 0.001$).

■ ASSOCIATED CONTENT

Supporting Information

The Supporting Information is available free of charge at https://pubs.acs.org/doi/10.1021/acsomega.3c01665.

NMR, HRMS, and FTIR spectra for compounds (PDF)

■ AUTHOR INFORMATION

Corresponding Authors

Peng Zhao − *NMPA Key Laboratory for Research and Evaluation of Drug Metabolism & Guangdong Provincial Key Laboratory of New Drug Screening, School of Pharmaceutical Sciences, Southern Medical University, Guangzhou 510515, People's Republic of China;* orcid.org/0000-0003-4377-1035; Email: smuzp@smu.edu.cn

Ling Lu − *NMPA Key Laboratory for Research and Evaluation of Drug Metabolism & Guangdong Provincial Key Laboratory of New Drug Screening, School of Pharmaceutical Sciences, Southern Medical University, Guangzhou 510515, People's Republic of China;* orcid.org/0009-0003-2728-0583; Email: linglu@smu.edu.cn

Authors

Junyu Liang − *NMPA Key Laboratory for Research and Evaluation of Drug Metabolism & Guangdong Provincial Key Laboratory of New Drug Screening, School of Pharmaceutical Sciences, Southern Medical University, Guangzhou 510515, People's Republic of China*

Xiaodong Tang − *NMPA Key Laboratory for Research and Evaluation of Drug Metabolism & Guangdong Provincial Key Laboratory of New Drug Screening, School of Pharmaceutical Sciences, Southern Medical University, Guangzhou 510515, People's Republic of China;* orcid.org/0000-0002-0051-105X

Shanhe Wan − *NMPA Key Laboratory for Research and Evaluation of Drug Metabolism & Guangdong Provincial Key Laboratory of New Drug Screening, School of Pharmaceutical Sciences, Southern Medical University, Guangzhou 510515, People's Republic of China*

Jiayin Guo − *NMPA Key Laboratory for Research and Evaluation of Drug Metabolism & Guangdong Provincial Key Laboratory of New Drug Screening, School of Pharmaceutical Sciences, Southern Medical University, Guangzhou 510515, People's Republic of China*

Complete contact information is available at: https://pubs.acs.org/10.1021/acsomega.3c01665

Author Contributions

†J.L. and X.T. contributed equally to this work.

Notes

The authors declare no competing financial interest.

■ ACKNOWLEDGMENTS

This work was finically supported by the National Natural Science Foundation of China (31100685).

■ REFERENCES

(1) Sarhene, M.; Ni, J. Y.; Duncan, E. S.; Liu, Z.; Li, S.; Zhang, J.; Guo, R.; Gao, S.; Gao, X.; Fan, G. Ginsenosides for cardiovascular diseases; update on pre-clinical and clinical evidence, pharmacological effects and the mechanisms of action. *Pharmacol. Res.* **2021**, *166*, 105481.

(2) Lee, J. I.; Park, K. S.; Cho, I. H. Panax ginseng: a candidate herbal medicine for autoimmune disease. *J. Ginseng Res.* **2019**, *43*, 342−348.

(3) Ko, E.; Park, S.; Lee, J. H.; Cui, C. H.; Hou, J.; Kim, M. H.; Kim, S. C. Ginsenoside Rh2 Ameliorates Atopic Dermatitis in NC/Nga Mice by Suppressing NF-kappaB-Mediated Thymic Stromal Lym-

phopoietin Expression and T Helper Type 2 Differentiation. *Int. J. Mol. Sci.* **2019**, *20*, 6111.
(4) Lee, H.; Lee, S.; Jeong, D.; Kim, S. J. Ginsenoside Rh2 epigenetically regulates cell-mediated immune pathway to inhibit proliferation of MCF-7 breast cancer cells. *J. Ginseng Res.* **2018**, *42*, 455−462.
(5) Lv, Q.; Rong, N.; Liu, L. J.; Xu, X. L.; Liu, J. T.; Jin, F. X.; Wang, C. M. Antitumoral Activity of (20R)-and (20S)-Ginsenoside Rh2 on Transplanted Hepatocellular Carcinoma in Mice. *Planta Med.* **2016**, *82*, 705−711.
(6) Qi, L. W.; Wang, C. Z.; Yuan, C. S. Ginsenosides from American ginseng: chemical and pharmacological diversity. *Phytochemistry* **2011**, *72*, 689−699.
(7) Gao, Q. R.; Zheng, J. H. Ginsenoside Rh2 inhibits prostate cancer cell growth through suppression of microRNA-4295 that activates CDKN1A. *Cell Proliferation* **2018**, *51*, No. e12438.
(8) Wang, C. Q.; He, H.; Dou, G. J.; Li, J.; Zhang, X. M.; Jiang, M. D.; Li, P.; Huang, X. B.; Chen, H. X.; Li, L.; et al. Ginsenoside 20(S)-Rh2 Induces Apoptosis and Differentiation of Acute Myeloid Leukemia Cells: Role of Orphan Nuclear Receptor Nur77. *J. Agric. Food Chem.* **2017**, *65*, 7687−7697.
(9) Yang, Z. Q.; Zhao, T. T.; Liu, H. L.; Zhang, L. D. Ginsenoside Rh2 inhibits hepatocellular carcinoma through beta-catenin and autophagy. *Sci. Rep.* **2016**, *6*, 19383.
(10) Guo, X. X.; Li, Y.; Sun, C.; Jiang, D.; Lin, Y. J.; Jin, F. X.; Lee, S. K.; Jin, Y. H. p53-dependent Fas expression is critical for Ginsenoside Rh2 triggered caspase-8 activation in HeLa cells. *Protein Cell* **2014**, *5*, 224−234.
(11) Li, B. H.; Zhao, J. O.; Wang, C. Z.; Searle, J.; He, T. C.; Yuan, C. S.; Du, W. Ginsenoside Rh2 induces apoptosis and paraptosis-like cell death in colorectal cancer cells through activation of p53. *Cancer Lett.* **2011**, *301*, 185−192.
(12) Oh, M.; Choi, Y. H.; Choi, S.; Chung, H.; Kim, K.; Kim, S. I.; Kim, D. K.; Kim, N. D. Anti-proliferating effects of ginsenoside Rh2 on MCF-7 human breast cancer cells. *Int. J. Oncol.* **1999**, *14*, 869−875.
(13) Li, M.; Zhang, D.; Cheng, J.; Liang, J.; Yu, F. RETRACTED: Ginsenoside Rh2 inhibits proliferation but promotes apoptosis and autophagy by down-regulating microRNA-638 in human retinoblastoma cells. *Exp. Mol. Pathol.* **2019**, *108*, 17−23.
(14) Hwang, H. J.; Hong, S. H.; Moon, H. S.; Yoon, Y. E.; Park, S. Y. Ginsenoside Rh2 sensitizes the anti-cancer effects of sunitinib by inducing cell cycle arrest in renal cell carcinoma. *Sci. Rep.* **2022**, *12*, 19752.
(15) Li, H.; Huang, N.; Zhu, W.; Wu, J.; Yang, X.; Teng, W.; Tian, J.; Fang, Z.; Luo, Y.; Chen, M.; et al. Modulation the crosstalk between tumor-associated macrophages and non-small cell lung cancer to inhibit tumor migration and invasion by ginsenoside Rh2. *BMC Cancer* **2018**, *18*, 579.
(16) Guan, N.; Huo, X.; Zhang, Z.; Zhang, S.; Luo, J.; Guo, W. Ginsenoside Rh2 inhibits metastasis of glioblastoma multiforme through Akt-regulated MMP13. *Tumor Biol.* **2015**, *36*, 6789−6795.
(17) Wang, Y. S.; Li, H.; Li, Y.; Zhang, S.; Jin, Y. H. (20S)G-Rh2 Inhibits NF-κB Regulated Epithelial-Mesenchymal Transition by Targeting Annexin A2. *Biomolecules* **2020**, *10*, 528.
(18) Huang, Y.; Huang, H.; Han, Z.; Li, W.; Mai, Z.; Yuan, R. Ginsenoside Rh2 Inhibits Angiogenesis in Prostate Cancer by Targeting CNNM1. *J. Nanosci. Nanotechnol.* **2019**, *19*, 1942−1950.
(19) Won, H. J.; Kim, H. I.; Park, T.; Kim, H.; Jo, K.; Jeon, H.; Ha, S. J.; Hyun, J. M.; Jeong, A.; Kim, J. S.; et al. Non-clinical pharmacokinetic behavior of ginsenosides. *J. Ginseng Res.* **2019**, *43*, 354−360.
(20) Hou, J.; Xue, J.; Zhao, X.; Wang, Z.; Li, W.; Li, X.; Zheng, Y. Octyl ester of ginsenoside compound K as novel anti-hepatoma compound: Synthesis and evaluation on murine H22 cells in vitro and in vivo. *Chem. Biol. Drug Des.* **2018**, *91*, 951−956.
(21) Chen, F.; Deng, Z. Y.; Zhang, B.; Xiong, Z. X.; Zheng, S. L.; Tan, C. L.; Hu, J. N. Esterification of Ginsenoside Rh2 Enhanced Its Cellular Uptake and Antitumor Activity in Human HepG2 Cells. *J. Agric. Food Chem.* **2016**, *64*, 253−261.
(22) Zhang, B.; Ye, H.; Zhu, X. M.; Hu, J. N.; Li, H. Y.; Tsao, R.; Deng, Z. Y.; Zheng, Y. N.; Li, W. Esterification Enhanced Intestinal Absorption of Ginsenoside Rh2 in Caco-2 Cells without Impacts on Its Protective Effects against H2O2-Induced Cell Injury in Human Umbilical Vein Endothelial Cells (HUVECs). *J. Agric. Food Chem.* **2014**, *62*, 2096−2103.
(23) Fu, B. D.; Bi, W. Y.; He, C. L.; Zhu, W.; Shen, H. Q.; Yi, P. F.; Wang, L.; Wang, D. C.; Wei, X. B. Sulfated derivatives of 20(S)-ginsenoside Rh2 and their inhibitory effects on LPS-induced inflammatory cytokines and mediators. *Fitoterapia* **2013**, *84*, 303−307.
(24) Fei, Z. L.; Liu, B. J.; Zhu, M. F.; Wang, W.; Yu, D. Antibacterial finishing of cotton fabrics based on thiol-maleimide click chemistry. *Cellulose* **2018**, *25*, 3179−3188.
(25) Schmid, B.; Warnecke, A.; Fichtner, I.; Jung, M.; Kratz, F. Development of albumin-binding camptothecin prodrugs using a Peptide positional scanning library. *Bioconjugate Chem.* **2007**, *18*, 1786−1799.
(26) Sivandzade, F.; Bhalerao, A.; Cucullo, L. Analysis of the Mitochondrial Membrane Potential Using the Cationic JC-1 Dye as a Sensitive Fluorescent Probe. *Bio-Protoc.* **2019**, *9*, No. e3128.
(27) Liu, Y.; Dong, X.; Wang, W.; You, L.; Yin, X.; Yang, C.; Sai, N.; Leng, X.; Ni, J. Molecular Mechanisms of Apoptosis in HepaRG Cell Line Induced by Polyphyllin VI via the Fas Death Pathway and Mitochondrial-Dependent Pathway. *Toxins* **2018**, *10*, 201.

https://doi.org/10.1021/acsomega.3c01665
ACS Omega 2023, 8, 17245−17253